RESEARCH ARTICLE

Macromolecular Rapid Communications
www.mrc-journal.de

Probing the Linear-to-Plastic Transition in Polymer Nanocomposites via Atomistic Simulations: The Role of Interphases

Hilal Reda, Panayiota Katsamba, Anthony Chazirakis, and Vagelis Harmandaris**

Polymer nanocomposites have found ubiquitous use across diverse industries, attributable to their distinctive properties and enhanced mechanical performance compared to conventional materials. Elucidating the elastic-to-plastic transition in polymer nanocomposites under diverse mechanical loads is paramount for the bespoke design of materials with desired mechanical attributes. In the current work, the elastic-to-plastic transition is probed in model systems of polyethylene oxide (PEO) and silica, SiO_2, nanoparticles, through detailed atomistic molecular dynamics simulations. This comprehensive, multi-scale analysis unveils pivotal markers of the elastic-to-plastic transition, highlighting the quintessential role of microstructural and regional heterogeneities in density, strain, and stress fields, featuring the polymer-nanoparticle interphase region. At the atomic level, the behavior of polymer chains interacting with nanoparticle surfaces is traced, differentiating between free and adsorbed chains, and identifying the microscopic origins of the linear-to-plastic transition. The mechanical behavior of subregions are characterized within the PEO/SiO_2 nanocomposites, focusing on the interphase and bulk-like polymer areas, probing stress heterogeneities and their decomposition into various force contributions. At the inception of plasticity, a disruption is discerned in isotropy of the polymeric density field, the emergence of low-density regions, and microscopic voids/cavities within the polymer matrix concomitant with a transition of adsorbed chains to free. The yield strain also emerges as an inflection point in the local versus global strain diagram, demarcating the elastic limit, and the plastic regime shows pronounced strain heterogeneities. The decomposition of the atomic Virial stress into bonded and non-bonded interactions indicates that the rigidity of the material is primarily governed by non-bonded interactions, significantly influenced by the volume fraction of the nanoparticle. These findings emphasize the importance of the microstructural and micromechanical environment at the polymer-nanoparticle interface on the linear-to-plastic transition, which is of great importance in the design of nanocomposite materials with advanced mechanical properties.

The ORCID identification number(s) for the author(s) of this article can be found under https://doi.org/10.1002/marc.202400612

DOI: 10.1002/marc.202400612

1. Introduction

Polymer nanocomposites have been widely adopted in various industrial sectors, such as automotive, aerospace, electronics, and packaging, due to their improved mechanical, thermal, and electrical properties. The mechanical and dynamical properties of glassy polymer nanocomposites (PNC), in particular, have been intensively studied over the last few decades, due to their scientific and technological importance.[1–5] Experimentally, insights into the mechanical properties of PNC, focusing on the elastic and plastic behavior, emphasizing the role of nanoparticle-matrix interactions and the influence of nanoparticle dispersion have been presented in the literature.[6–9] In addition to experiments, the mechanical properties of glassy polymer nanocomposites have been studied by molecular dynamics (MD) simulations in the linear elastic regime,[10–15] as well as under large deformation.[16–18] Glassy PNC exhibit a maximum in the stress-strain curves (yielding point) at a strain value of a few percent and a typical yield stress value of a few GPa,[19] followed by the so-called stress softening regime corresponding to a decrease of stress, depending on the thermo-mechanical history of the structures.[20] This regime is followed by a stress plateau corresponding to plastic flow or perfectly plastic behavior. The strain hardening may then occur at even larger strain values. This regime corresponds to an approximately linear increase in stress as a function of strain. Strain hardening, which is enhanced in PNCs with high molecular weights,[21–23] is essential to improve rigidity, as it prevents strain localization, and crack propagation.

The elastic-to-plastic transition transition of glassy bulk polymers has been investigated by MD simulations mostly via generic bead spring coarse-grained models. Robbins and co-workers provided new information on mechanisms related to strain hardening that focuses on large-scale chain relaxation without invoking entanglements.[24–27] MD simulations also report rapid segmental dynamics[28–32] during mechanical plastic deformation

that has elevated the potential energy landscape.[33,34] In addition, various models have been proposed to incorporate orientation-induced hardening behavior, usually employing the Lee–Kröner decomposition.[35,36]

A great deal of research has been carried out to investigate the mechanisms of yield during the deformation of glassy PNCs. Many experimental techniques, including mechanical tests,[37–40] NMR,[41] positron annihilation lifetime spectroscopy[42] and dielectric spectroscopy,[41,43] have been applied to acquire knowledge about molecular processes associated with the deformation and production of glassy polymers. These experiments indicate that segmental mobility can be considerably higher during external deformation beyond the yield point.

Furthermore, complementary to experimental studies, different theoretical models have been developed to explain yielding behavior and plasticity phenomena in PNCs.[21] Recently, a comprehensive force-level microscopic theory based on the nonlinear Langevin equation (NLE) has been developed.[44–46] Most of the theoretical work is based on the common idea that stress would lower the potential barrier and that plastic regimes can be reached through activation of vitreous segments. It is well known that yielding occurs when the segmental α relaxation time has become comparable to the experimental time scale, i.e., the reciprocal of the deformation rate. The Eyring-like idea of activation attempts to explain how plasticity emerges and cannot itself be seen to know when this mechanism ceases to work.[47]

In addition to the above work, unraveling the processes involved in the transition from elastic-to-plastic transition regions in PNCs by molecular dynamics simulations remains elusive, mainly for multi-component polymeric nanostructured materials. Computational approaches have been extensively used for predicting the mechanical behavior of PNCs, traditionally through continuum simulations and micromechanical models, but refer mostly to the linear regime.[13,48–54] Despite the fact that the aforementioned continuum models do not include information at the molecular scale and do not always predict the desired global properties with accuracy, they highlight the importance of many fundamental factors affecting macroscopic properties in PNCs, such as the polymer/nanoparticle interphase region and the importance of well-dispersed nanofillers.[55–60]

The polymer/nanofiller interface has received significant attention in the literature.[57,58,61–63] It is recognized that the properties of polymer chains in this regime could differ substantially from those of chains far from the nanofillers.[58,62,64–66] In general, polymer chains as the vicinity of interphases can be adsorbed, attached or depleted from the surfaces, and often exhibit significantly different properties from their bulk polymer counterparts, depending on the strength of the polymer/substrate, or polymer/nanofiller, interaction and the distance from the boundary surface of the nanofiller.[59,64,65,67–78] In general, it is well known that the width of the interphase depends on the property under study.[79] Typically the interfacial regions is defined via the mass density distribution of polymer chains in the vicinity of the nanofiller,[80–83] while the deviation of the local stress distribution and the gas solubility from the bulk behavior has been also used in the literature.[84] In this work, we examine the microscopic and atomistic origins of the elastic-to-plastic transition of amorphous polymer nanocomposites undergoing tensile deformation using a methodology centered on detailed atomistic molecular dynamics simulations, described in Section §2. In Section §3 we investigate markers across sub-region and atom/chain levels of description, analyzing the evolution of specific properties during deformation at various scales. In more detail, in Sections §3.2 and §3.1, we examine the evolution of the polymeric density profile with increasing tensile strain, probing the 3D microstructural details, and investigating emerging anisotropies and low-density regions at the transition. We connect the decrease in interphase region's density to the significant decrease of adsorbed chains, as these become free during the elastic-to-plastic transition. We further probe the conformational changes of polymer chains during deformation by computing the distribution of the vector connecting two consecutive monomers along the PEO chains, that is about the size of the Kuhn segment, focusing on changes in the elastic-to-plastic transition region. In Section §3.3, we examine the manifestations of the elastic-to-plastic transition in the local strain and stress fields of the interphase and matrix (bulk-like) sub-regions. At the onset of the elastic to plastic transition, the local (non-affine) strain field of local regions (interphase and matrix) deviates from its linear regime, as a result of the breakdown of the compatible deformation condition. This manifests itself as an inflection point in the local versus global strain diagram, which emerges as a marker of the yield point and the elastic-to-plastic transition. We further investigate the origin of the local stress in the interphase and matrix regions by computing its non-bonded and bonded contributions, and highlight their dependence on the volume fraction. We finish with conclusions and perspectives in Section §4.

2. Methods: Atomistic Model and Simulations

2.1. Generation and Equilibration of Model Systems

We have performed atomistic molecular dynamics (MD) simulations on PEO/SiO_2 model nanocomposites with varying volume percentages of silica nanoparticles (5 wt% ($\phi = 1.9$ vol%), 12 wt% ($\phi = 4.5$ vol%), 33 wt% ($\phi = 12.7$ vol%)). The primary focus of our results will be on the system with a volume fraction of ($\phi = 12.7$ vol%), as the qualitative properties observed are consistent across a wide range of volume fractions of nanoparticles. For properties where comparative analysis is crucial, we will include data from other volume fractions to provide a comprehensive understanding. The silica nanoparticles are amorphous, with an almost spherical shape and a radius of about 2 nm. The PEO chains are monodisperse, each one consisting of 50 monomers, that is, their molecular weight is about 2.2 kDa, being in the Rouse-like

H. Reda, P. Katsamba, V. Harmandaris
Computation-based Science and Technology Research Center
The Cyprus Institute
Aglantzia, Nicosia 2121, Cyprus
E-mail: h.reda@cyi.ac.cy; v.harmandaris@cyi.ac.cy
A. Chazirakis, V. Harmandaris
Institute of Applied and Computational Mathematics
Foundation for Research and Technology - Hellas
Heraklion GR-71110, Greece
V. Harmandaris
Department of Mathematics and Applied Mathematics
University of Crete
Heraklion GR-71110, Greece

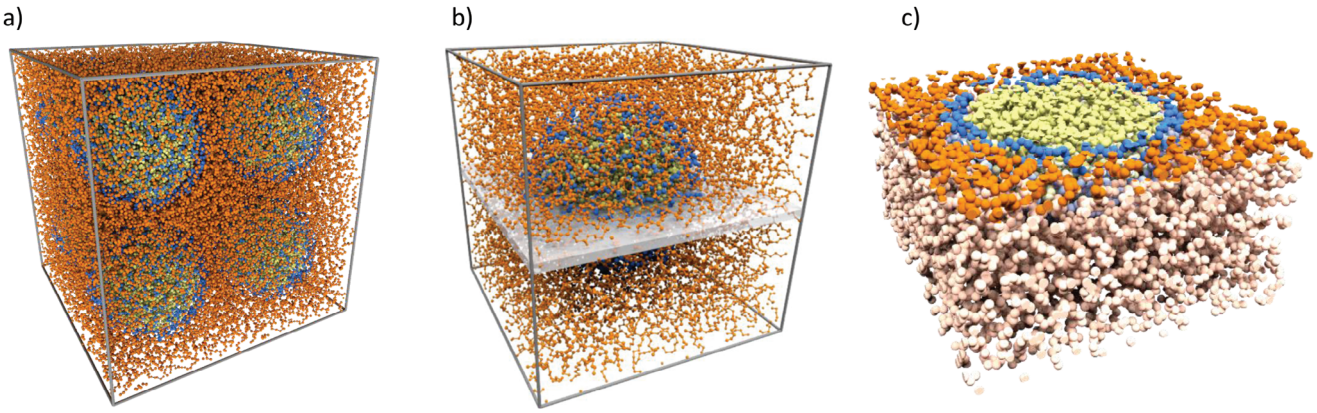

Figure 1. a) Snapshot of the atomistic PEO/SiO_2 model nanocomposite with $\phi = 12.7$ vol%, replicated along each direction taking into account the periodic boundary condition. The polymer/nanoparticle interphase is shown in blue, the polymer matrix region is shown in orange, and the silica nanoparticle is shown in yellow. b) Representative volume element of the model nanocomposite system consisting of one nanoparticle. c) A slice of thickness 6 Å passing through the center of NP is also shown with the relative distribution of atoms through the slice.

regime. More details on the molecular model of PEO and the SiO_2 nanoparticle can be found elsewhere.[85] For integrating the equations of motion, in all MD simulations a time step of 1 fs is used. Non-bonded interaction forces are truncated after a cut-off radius $r_{cut} = 1$ nm. Dispersion tail corrections are applied for the global energy and pressure, whereas periodic boundary conditions are applied in all directions.

The model glassy PEO/SiO_2 systems are obtained via the following procedure: 1) First, several (here five) independent, uncorrelated, and well-equilibrated atomistic configurations are obtained at a high temperature ($T = 400$ K) via long (a few μs) atomistic MD simulations.[85] To prepare the high-temperature configurations, we first inserted the polymer chains into a large simulation box containing one silica nanoparticle. After energy minimization, a long *NPT* equilibration run was performed to compress the box and then equilibrate the density and conformations of the polymer chains in the sample. To ensure reaching an equilibrated structure, the length of the equilibration run (after compression of the box) was longer than the average relaxation time of the end-to-end vector of the chains in the sample; 2) Atomistic model systems are then cooled well below T_g, with a cooling rate of 10 Kns^{-1} to 150 K, noting that the experimental T_g of the bulk PEO is around 220 K[86]; 3) After cooling, we finally perform additional MD runs on the system with many NPs for about 1 ns in order to allow for small-scale relaxation, before applying the deformation to the entire simulation box. The current size of the simulation boxes will be reported and then the volume fraction is calculated (**Figure 1**).

2.2. Atomistic Simulations of the Systems

After preparing the glassy PNC samples, we apply uniaxial deformation with a constant strain rate $\dot{\epsilon}_{xx} = 5 \times 10^{-5}$ fs^{-1}. Due to the isotropic behavior of the PNCs, a single applied deformation is sufficient to determine its overall mechanical properties. The deformation was performed using LAMMPS with the Nosé–Hoover thermostat and Parinello–Rahman barostat. We should also note that, in principle, the mechanical properties of the polymer nanocomposite depend on the arrangement of NPs within the polymer matrix. Here, we assume a scenario of well-dispersed NPs in which silica NPs are in a simple, cubic-like arrangement within the polymer matrix, i.e., there is no aggregation of the nanoparticles. The overall applied deformation considered was up to 0.6, but, in the current work, we focus primarily on the linear elastic regime. Here we note that the applied uniaxial deformation of the box respects the periodic boundary conditions along the axis of deformation; i.e., for each time the box size or shape is changed, the atom positions are remapped to the new box via the periodic boundary conditions.

2.3. Calculation of Local Strain and Stress Field

To investigate the spatial distribution of the (local) mechanical properties of the model polymer nanocomposite systems, we calculated the stress and strain at the atomic level resolution. For this, we compute the value of the stress per atom (local stress) given by the atomic Virial formalism. Concerning the local strain, we utilize a recently proposed methodology to directly probe the strain field in model polymer nanocomposites at the atomic level.[87] At the initial stage, the deformation gradient for each atom is calculated through a minimization problem related to the position of the atom of interest to its neighboring atoms within the cutoff radius r_{cut}, thus allowing probing the distribution of the (local) strain fields in the atomistic model using the definition of the Lagrange Green strain tensor with respect to the reference coordinates. More information on the computation of the local strain can be found in our previous work.[15,55,87]

3. Results and Discussion

3.1. Evolution of Adsorbed and Free Polymer Chain Populations During Deformation

We start by investigation the behavior of the various conformations of PEO chains in the vicinity of the silica nanoparticle in

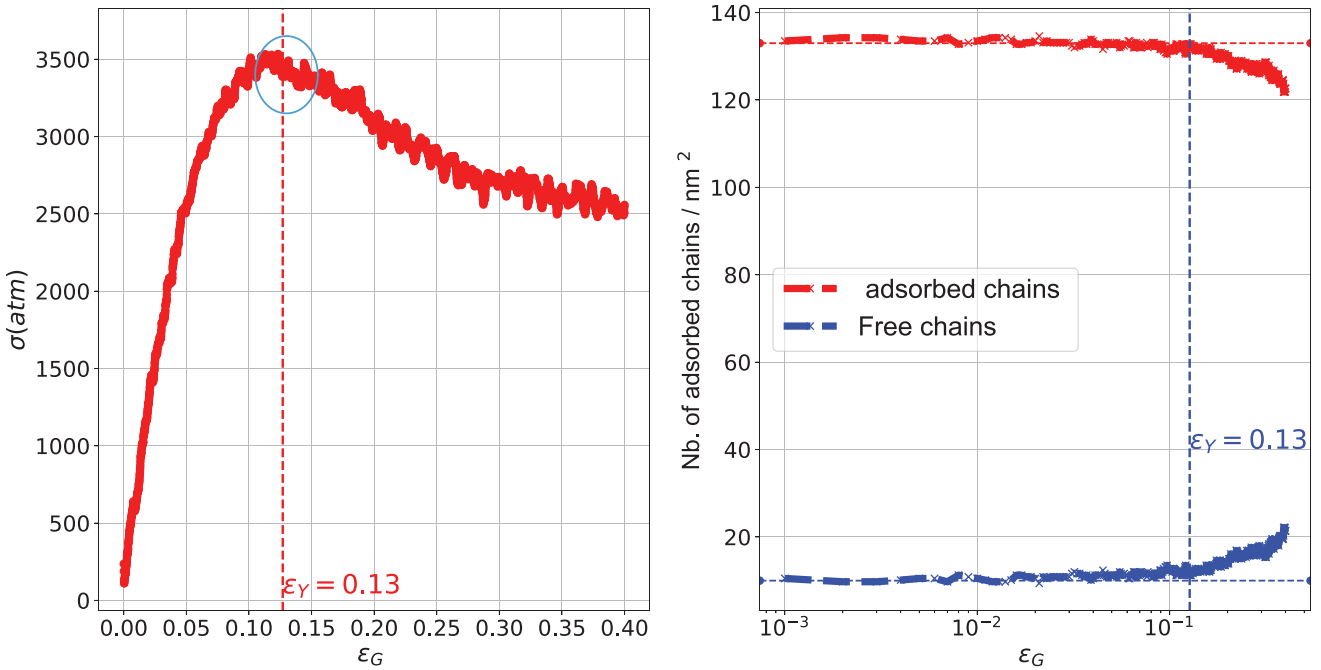

Figure 2. a)Global stress (σ)–strain (ϵ) curve for PNC, b) Number of adsorbed and free chains as a function of tensile deformation.

the elastic-to-plastic transition region. We classify chains or segments as free or adsorbed chains, the latter defined as chains having at least one atom within the interphase region (details about the width of the interphase are given in Figure 4a).

We first investigate the influence of strain on the number of adsorbed chains within the PNC system (**Figure 2**). For this analysis, we compare the global/macroscopic manifestations of the mechanical response given by the global stress (σ) – strain (ϵ) diagram in Figure 2a, with the atomistic/chain level description, plotting the evolution of the number of adsorbed/free chains as a function of strain, plotted in Figure 2b. The stress versus strain diagram in Figure 2a, shows an initial increase almost linear as expected in the elastic regime, followed by a drop occurring at yield strain of approximately $\epsilon_Y = 0.13$, which is a clear indication of the plastic transition. The region after this peak is referred to as strain softening of the material due to the much-reduced stress response of the material at these larger strains.

In Figure 2b, we highlight the significant reduction in the number of adsorbed chains and the concurrent significant increase in the number of free chains, both of which occur at strain 0.13. Thus, plasticity at the polymer/nanofiller interphases is strongly correlated with the decrease in the number of adsorbed chains.

During the elastic regime, the stable behavior of the polymer chains is reflected by the number of adsorbed chains remaining constant until a critical strain $\epsilon = 0.13$ (Figure 2). The critical value of the yield strain upon which the number of adsorbed chains changes is in excellent agreement with the classic marker of the elastic-to-plastic transition, which is the yield point shown as the peak of the global stress-strain diagram for the entire material in Figure 2a. Beyond the yield-strain ($\epsilon > \epsilon_Y$), in the plastic deformation regime, the number of adsorbed chains decreases, leading to an increase in the number of free chains. Thus, permanent deformation occurs when the conformation of the polymer chains changes. The above data signify the number of adsorbed chains as a definite marker of the elastic-to-plastic transition, which also allows us to attribute these plasticity structural changes to the de-adsorption of chains from the NP, i.e., adsorbed chains becoming free.

The discussion above emphasizes the important role of the microstructure and polymer chain behavior in the mechanical behavior of PNCs during the elastic-to-plastic transition. We further examine the importance of the chain microstructure by analyzing the distribution of the length of Kuhn segments. Given that for PEO the Kuhn segment is about $l_k \approx 1nm$, and the monomers have an approximate length of 4.5 Å, we compute the distribution of the length of vectors connecting two consecutive monomers along the PEO chains (2-mer length), $P(l_k)$, and how it changes during deformation in **Figure 3**). Figure 3 presents the standard deviation of the 2-mer length and its probability distribution function $P(l_k)$ for a wide range of global strain values (inset). It is interesting that as the applied global strain increases, the standard deviation of the 2-mer length manifests transitions between different behaviors, which also coincide with the critical values observed using the strain value markers discussed above (ϵ_y = 0.1).

3.2. Evolution of the Atomic Mass Density Profile During Deformation

Central to our analysis of the model PEO/SiO_2 nanocomposites, is the interphase region between the polymer (PEO) and the nanofiller (SiO_2) phases. We define the width of the PEO/SiO_2 interphase by computing the mass polymer density as a function of the distance from the center of the SiO_2 nanoparticle, ρ_{eff}, at

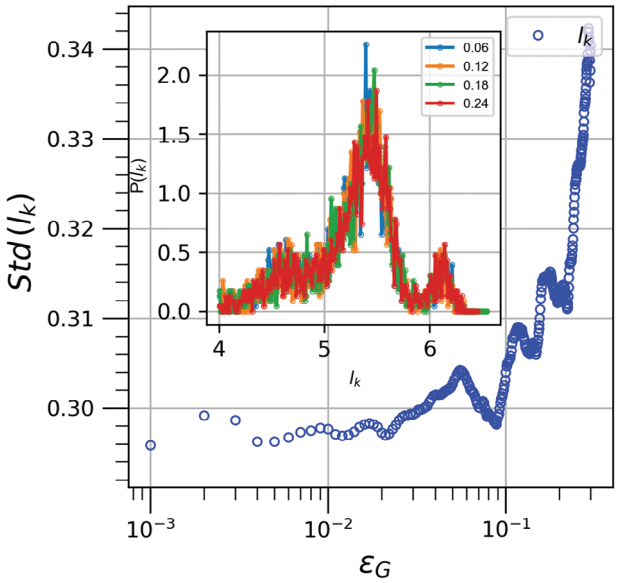

Figure 3. Standard deviation of the 2-mer length changes during deformation. (Inset) Probability distribution of the 2-mer length for strain values in the elastic-to-plastic transition. We quantify the lengths of the segments as multiples of the Kuhn length, l_k, Noting that in our case the Kuhn length $l_k \approx 1$ nm, and the monomers have an approximate length of 4.5 Å, means that one Kuhn length includes approximately two monomers.

equilibrium, i.e., before applying any tensile strain. Data about the ρ_{eff} are shown in **Figure** 4a. We calculate the width of the interphase region as the distance from the outer surface of the SiO_2 nanoparticle up to the first minimum of the density profile, which is about $l_s = 5.5$ Å.

Figure 4a shows the evolution of the polymer density profile ρ_{eff}, under deformation, at different strain values between 0.06 and 0.18. The simulation results are analyzed as a function of the radial distance from the center of mass of the silica NP, using a binning of 0.6 Å. Regimes of high and low polymeric mass densities are observed at small distances (around 5 Å from the outer surface of the nanoparticle) similar to the equilibrium profile discussed above.

It is of interest that the width of the interphase does not vary much with the imposed strain. At the same time, the first peak in the density profile corresponds to atoms belonging to the interphase region next to the surface of the NP, while the secondary peak in the density profile is attributed to atoms belonging to polymer chains in the matrix region.

As the strain increases, the first peak of the density profiles is kept approximately constant for strains within the elastic region; however, once the strain increases beyond the point of plastic behavior, this first peak in the density profile drops significantly, as expected, because of the exit of atoms from this interphase region as atoms detach from the surface of the NP. The decrease in the effective mass density of the polymer region after the first peak in Figure 4a is naturally related to the increase in the corresponding volume of the simulation box.

Figure 4b shows the angular distribution of the density within the the interphase region, demonstrating the initial axisymmetry at equilibrium and the anisotropy induced by the tensile strain along the prescribed axis. When the system is in equilibrium $\epsilon = 0$, the density in the interphase region is almost axisymmetric; that is, the distribution of polymer chains is uniform and independent of angular position θ. During elastic ($\epsilon = 0.1$) or plastic deformation ($\epsilon = 0.3$), the density profile gradually loses its axisymmetry and becomes dependent on the direction of the applied load. The description of the density profile being symmetric around $\theta = 90$ is indicative of how the material deforms under stress. In the $\theta = 0$ and $\theta = 180$ directions, corresponding to the axis of the applied deformation, the density decreases with increasing strain, due to local tensile stretching. Under tensile deformation, the local density is maximized at $\theta = 90$, that is, the direction perpendicular to the applied deformation. This is due to the Poisson's effect, as the material is stretched in the $\theta = 0$, 180 direction, and it contracts in the perpendicular, $\theta = 90$, direction. This lateral contraction results in a local increase in density since the system is being compressed because of the effect of the Poisson's ratio. The observed asymmetry in the density profile in the matrix region for ($\epsilon = 0.3$) in Figure 4c, attributed to the decrease in the average density and the void formation during plastic deformation, highlights the different behaviors between the interphase and matrix regions during the transition from elastic to plastic regions.

During deformation, the imposed uni-axial tensile strain is expected to disrupt the isotropic, spherical symmetry of the polymer density that was present at equilibrium as observed in Figure 4. In order to further investigate the distribution of the 3D local density throughout the simulation box, we plot heat maps of the local polymeric density within slices of the simulation box in **Figure** 5. We do so for a slice that passes through the center of the NP (top sub-plots), and one through the polymer matrix region (bottom-sub-plots), at a distance of about 22.5 Å from the center of the silica nanoparticle. We present the evolution of the polymeric density in these two slices at equilibrium (left sub-plots), at a strain $\epsilon = 0.06$ of elastic deformation (middle sub-plots) and at a higher strain $\epsilon = 0.3$ of plastic deformation (right sub-plots).

As expected, in regions close to the corners of the (cubic) simulation box, which are further away from the surface of the nanoparticle, the polymeric density is nearly identical to that of a pure homogeneous, neat polymer (without silica) system.

The disruption of spherical symmetry in the polymeric density becomes apparent only in the plastic regime, with the emergence of a new low-density region and microscopic voids or cavities within the polymer matrix. We attribute this emergent anisotropy primarily to the development of non-affine deformation patterns within the PNC, and resulting localized changes in the density distribution which disrupt the spherical symmetry of the density profile observed in the elastic region. The emergence of microscopic cavities and/or voids within the polymer matrix during plastic deformation contributes to local density reductions and can significantly affect the mechanical properties of the material.

3.3. Local Strain and Stress in the Interphase and Matrix Sub-Regions

We now turn to a regional-level characterization of the spatial distribution of stress-strain properties in these heterogeneous PEO/SiO_2 systems. We investigate how the elastic-to-plastic transition manifests at this "local" level, within specific domains, by

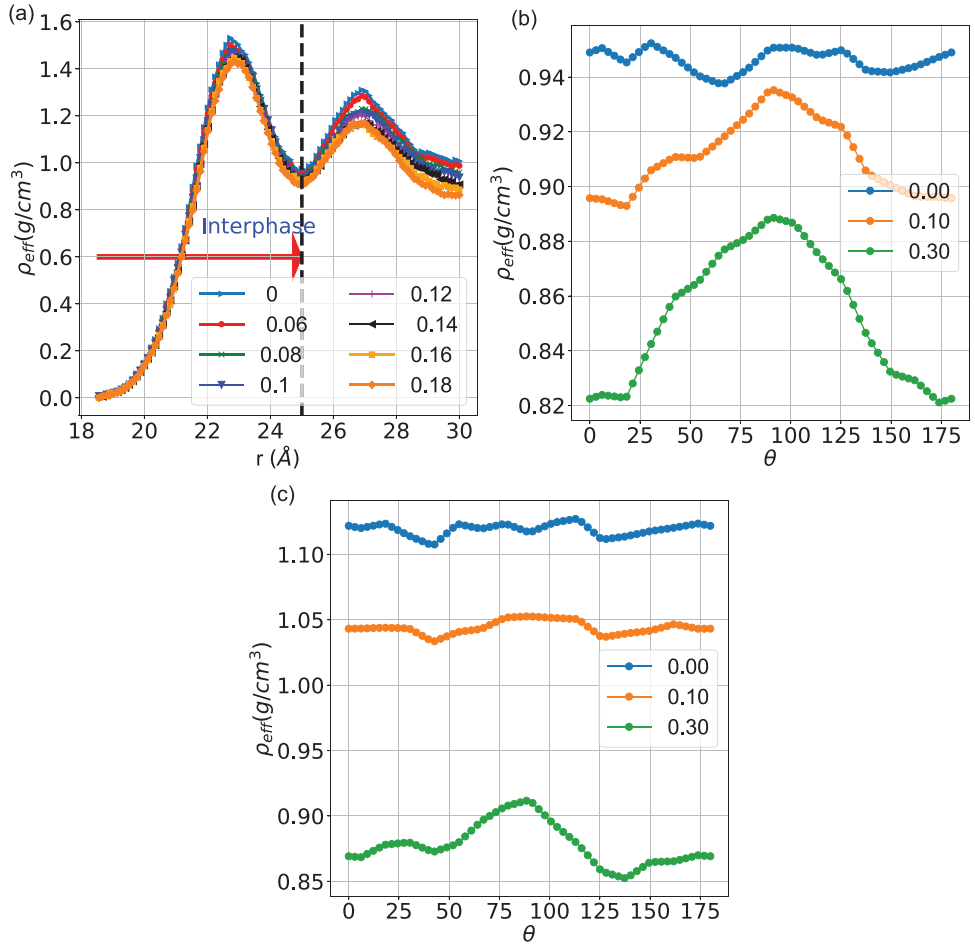

Figure 4. a) Evolution of the PEO atomic mass density profile as a function of the radial distance from the center of SiO_2 NP, for different strain values. b) Angular distribution of the density in the interphase region for three different deformations. c) Angular distribution of the density in the matrix region for three different deformations. Angles are given in degrees.

making a distinction between the polymer chains within the polymer/nanoparticle interphase region (defined in Section §3.2 as having thickness 5.5 Å based on the first peak of the density profile) and in the matrix region, i.e., the remaining polymer region considered as bulky.

Figure 6a shows the local deformation (strain), averaged within the interfacial and matrix regions, as functions of the applied deformation steps (global deformation), throughout the applied tensile deformation.

We first note that the local deformation does not exactly follow global deformation, i.e., the deformation occurring is non-affine due to the heterogeneity of the PNC, with less deformation in the interphase region than in the polymer matrix, as expected by the interaction of the interphase with the rigid silica nanoparticle. We highlight the emergence of an inflection point in the average of local strain observed in both sub-regions, beyond which the material exits the linear elastic regime of low strain. The inflection point emerges as a novel marker of the elastic-to-plastic transition, representing the yield strain (limit of elastic regime) for each region connected with the breakdown of the compatible deformation condition. We note that to locate the inflection point, the local strain data in each region were fitted linearly (indicated by the dashed lines in Figure 6a) in two windows $\epsilon \in (0, 0.15)$ and $\epsilon \in (0.17, 0.4)$ for the matrix region while $\epsilon \in (0, 0.18)$ and $\epsilon \in (0.15, 0.4)$ for the interphase region.

As is clear from Figure 6a in the elastic region of the bulk system ($\epsilon < \epsilon_Y = 0.1$), the average local deformation matches exactly the global deformation, indicating that the deformation of the material is almost affine. We highlight the emergence of a critical strain $\epsilon_Y = 0.12$ beyond which the average local strain within the bulk system departs from this linear behavior, and we associate this with the exit of the material from the low-strain linear elastic regime and the entry into the strain softening regime.

The corresponding stress–strain data for both sub-regions shown in Figure 6b exhibit an initial linear elastic behavior for low strains followed by a departure from the linear elastic regime manifested by a significant drop and strain softening behavior that is characteristic of the elastic-to-plastic deformation. As expected, the interphase, being much stiffer than the matrix region, presents a higher gradient in its stress-strain diagram in the linear regime. We highlight the values of the local yield strain for the interphase region, as extracted from the inflection point of the local regional versus global strain in Figure 6a.

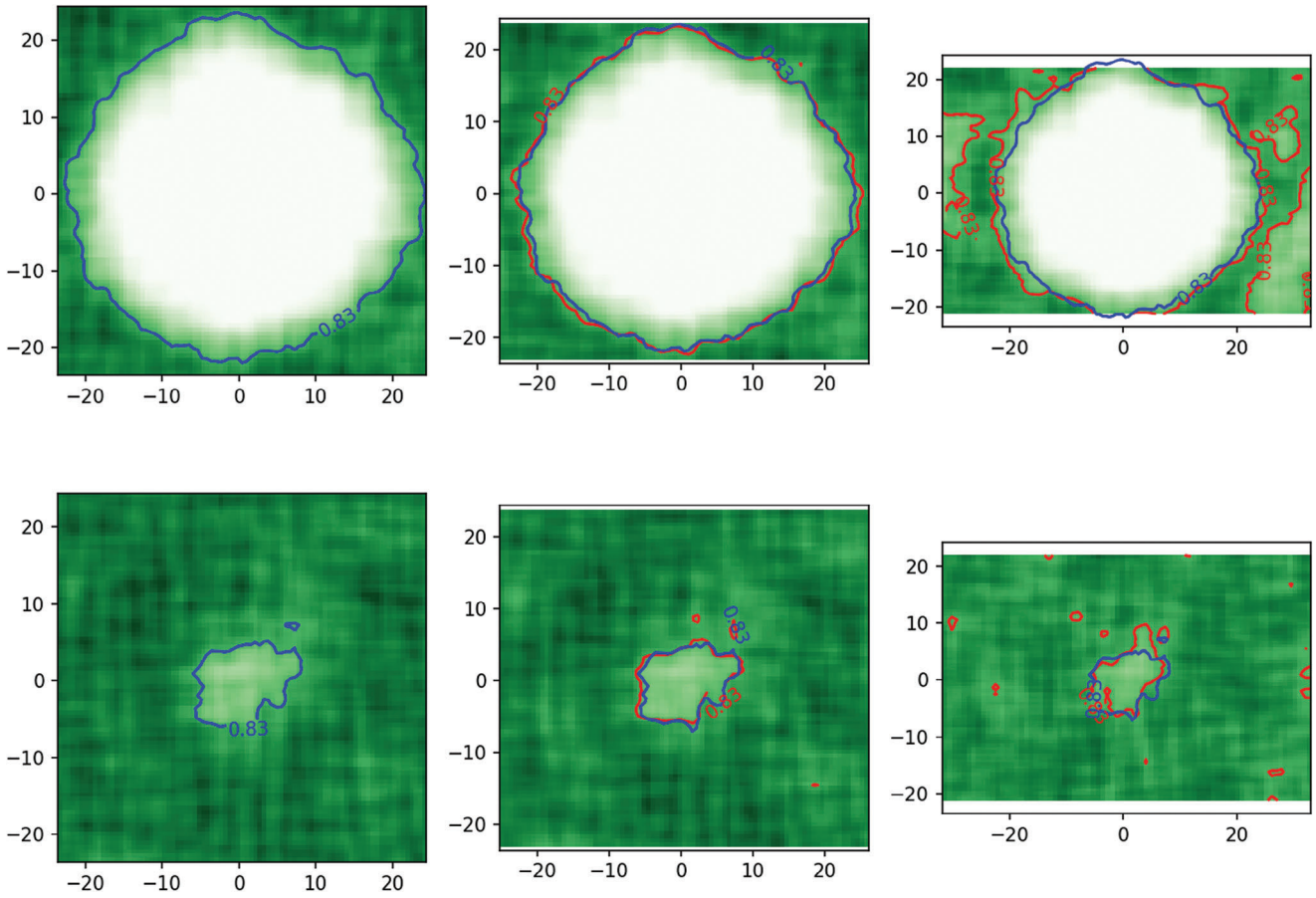

Figure 5. 3D mass density profile of PEO chains within a plane (disk) passing through the center of the silica nanoparticle (top) and at distance 22.5 Å from the center of nanoparticle at equilibrium, during elastic deformation ($\epsilon = 0.06$) and plastic deformation ($\epsilon = 0.3$) respectively.

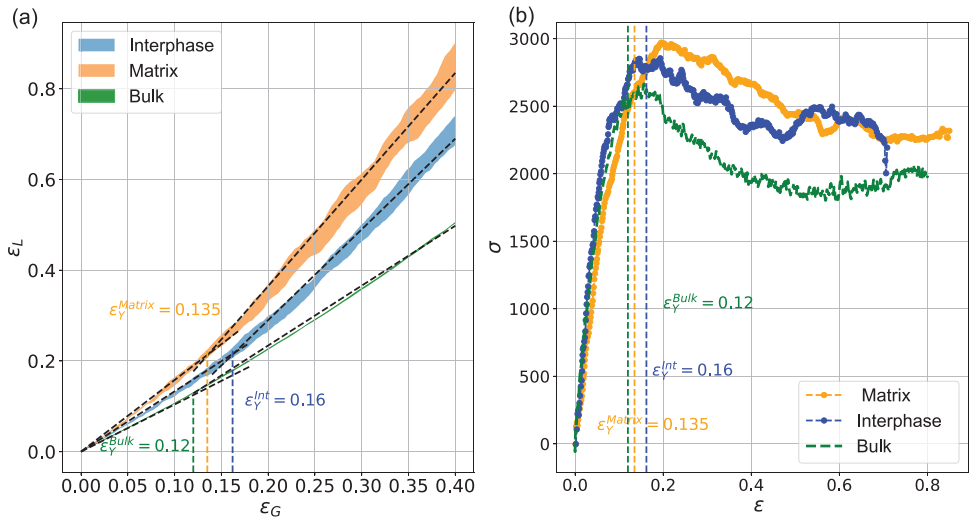

Figure 6. a) Evolution of the average local strain in interphase and matrix region during deformation, b) Stress–Strain diagram for both regions with the corresponding yield strain.

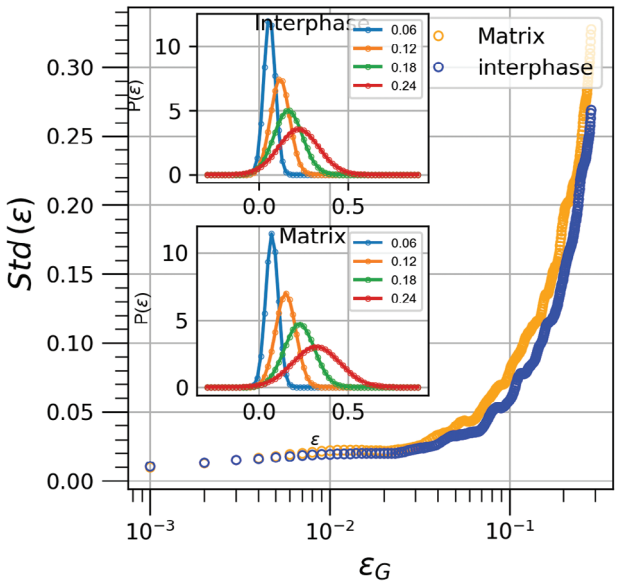

Figure 7. Standard deviation of local strain within the Matrix and Interphase region. (Inset) Probability distribution of local deformation for r strain values in the elastic-to-plastic transition.

In **Figure 7** we present the probability distribution functions (inset) and the associated standard deviations of the local strain, P(ϵ), in the interphase and matrix regions, for a wide range of global strain values in the elastic and plastic regimes. We observe that the distributions for the local strain are symmetric (resembling Gaussian ones), starting off as narrow peaks in the linear regime and becoming progressively broader at higher strains, thus marking a more heterogeneous strain field as strain increases for both regions; interphase and matrix. The standard deviation of P(ϵ) reflects the strong heterogeneities of the local strain. We highlight the onsets of different trends observed at the transition strain values of around 0.1 for both regions, in remarkable agreement with the previous markers of the elastic-to-plastic transition discussed above. In addition, the standard deviation of P(ϵ) in the matrix region is slightly higher than in the interphase.

3.3.1. Decomposition into Bonded versus Non-Bonded Interactions

Next, we investigate the role of different potential terms in the stress field during deformation. In **Figure 8** we compute both the bonded (bond, angle, and dihedral) and non-bonded interaction contributions in the atomic Virial part of the stress tensor. We observe that the general trend of the stress-strain diagrams for the non-bonded and bonded contributions follows a profile similar to that for the previous plots in Figure 8b, and the corresponding yield points are in approximate agreement. We also note that the non-bonded contribution in the interphase region is higher than the one in the matrix region because of the interaction between the nanoparticle and the adsorbed polymer atoms. On the contrary, the contribution of the bonded interaction to stress is found to be very similar in both regions. The presence of the non-bonded energy in the material improves its stiffness and makes it more rigid to resist deformation. This is clear from the slope of the curves, where the non-bonded energy had higher slope whereas the bonded energy had lower slope. The slight difference between the interphase and matrix contributions to the bonded energy in the low-strain region seen in Figure 8a, can be attributed to the higher strain experienced in the matrix region compared to the interphase (note that the contribution of bonded stress is expected to be the same). In addition, it is important to highlight some key points for comparison with the bulk system. The behavior observed in the PNC subdomains, mainly interphase and matrix, differs from that of the bulk, neat polymer, system. Specifically, there is a notable decrease in non-bonded stress in the plastic region for the bulk system, whereas the stress-strain curves for the interphase and matrix subdomains of PNC are similar to the global stress-strain curve. In the context of PEO-SiO_2 interactions, the differences in behavior between bonded energies and non-bonded energies (intermolecular forces, including interactions at interfaces) are critical. The presence of silica can alter these energies, influencing the stress distribution and energy dissipation during deformation. Non-affine deformation in PNC leads to non-uniform stress distributions, particularly in the interphase and matrix regions. This behavior significantly alters the contributions of non-bonded and bonded stresses in comparison to bulk polymer systems. This is mainly due to the change of the distances and angles between non-bonded atoms or molecules, affecting the interaction energy.

The contribution of the bonded and the nonbonded interactions to the atomic Virial stress within the matrix region depends strongly on the volume percentage. As the volume percentage of the filler decreases, the pair contribution to the Virial stress also decreases, i.e., the interaction between atoms of SiO_2 and PEO becomes less significant. For very low volume percentages, such as $\phi = 1.9\%$, the pair contribution to the Virial stress is closer to the value observed in the bulk material. This suggests that the filler has a diminishing impact on the stress distribution at low concentrations. The contribution of the bonded interactions to the Virial stress remains constant regardless of the volume percentage of the filler. This implies that the stress arising from the bonds between atoms belonging to the same molecules in PNC is not affected by the amount of filler present. Consequently, the pair contribution plays a significant role in determining the overall rigidity of PNC. The interactions between the polymer matrix and the nanofillers, particularly the interfacial interactions and dispersion of nanofillers, greatly influence the mechanical properties of the PNCs, including their rigidity. By optimizing these interactions, for example, through the functionalization of nanofillers, the overall rigidity and other mechanical properties of PNCs can be enhanced.

Next, we investigate in more detail the role of the bonded interactions energies in the global stiffening of the polymer during the tensile test, further decomposing the total bonded energy into bond, angle, dihedral, and improper contributions, shown in **Figure 9**. Bond stretching refers to stretching or compression of the bonds between atoms during deformation. The energy associated with it varies as the length of the bond deviates from its equilibrium value. By comparing the slopes of the four curves it is clear that bond stretching tends to have the most significant impact on the bonded energy where both interphase and matrix contributions are almost the same.

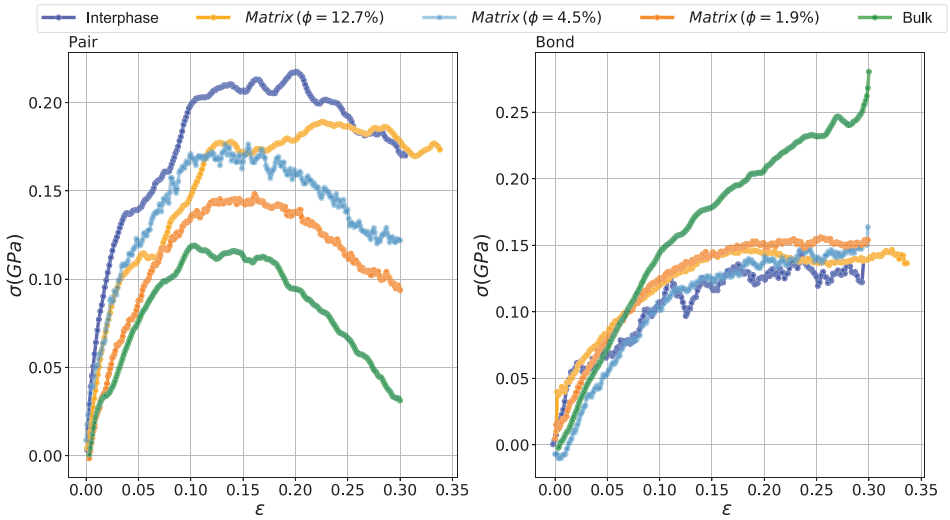

Figure 8. Average local stress in interphase and matrix regions (for different volume fraction) due to non-bonded (pair contribution) and bonded interactions during tensile deformation.

We observe that the general trend of the stress–strain diagram for the bonded contribution in each sub-region follows a profile similar to the data shown in Figure 6b. Bond angles describe the angles between adjacent bonds in a molecule. Although the bond angles contribute to the overall bonded energy, their influence is generally smaller than that of the bond stretching contribution. Meanwhile, the dihedral torsion represents the rotational freedom around the bond and their contribution here is very low compared to that of the others. Furthermore, we can observe from Figure 9 that the contribution of the improper terms is null to the global bond stress.

4. Conclusion and Perspectives

In this study, we have explored the microstructural underpinnings of the mechanical response of polymer nanocomposites undergoing imposed tensile strain and transitioning from elastic to the plastic response. Through detailed atomistic molecular dynamics simulations and multi-scale homogenization techniques on a model PEO/SiO_2 system, we have uncovered various markers signifying the elastic-to-plastic transition across different levels of description. Our hierarchical, multi-angle investigation has shed light on the critical role of microstructure and

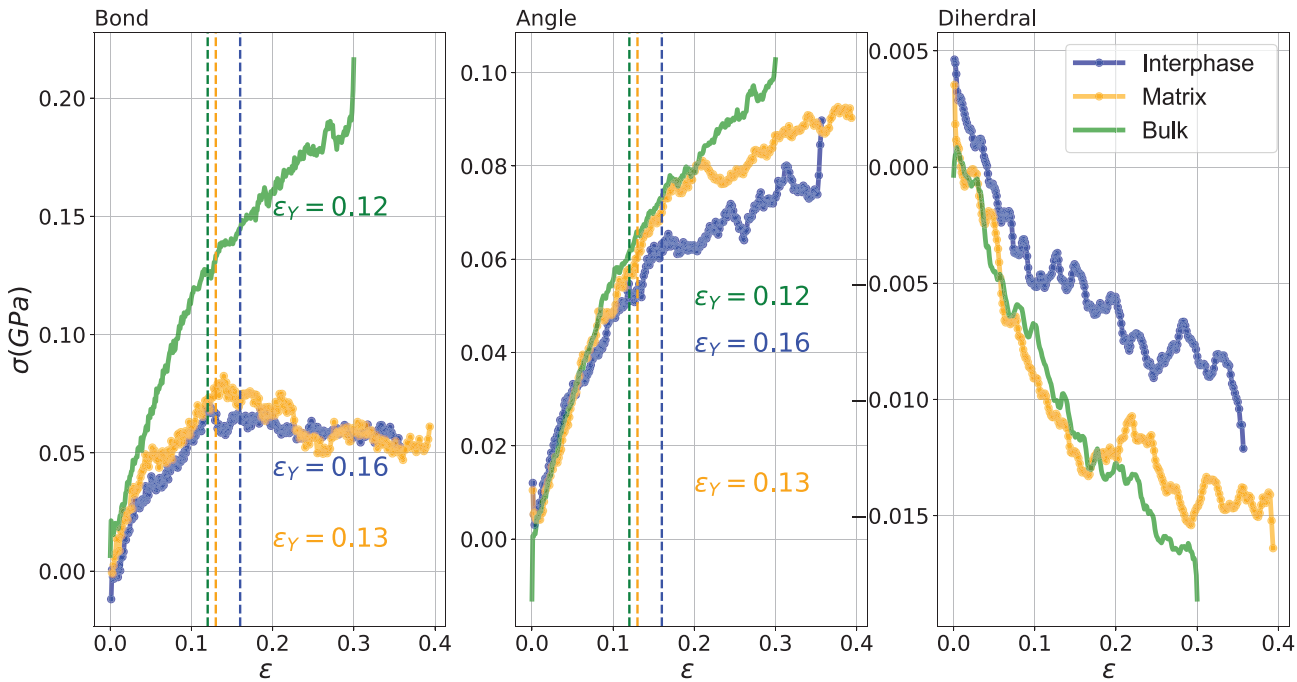

Figure 9. Contribution of bond, angle and dihedral interaction terms in the local stress for a PEO/SiO_2 system with ϕ = 12.7%.

regional heterogeneities in the density, strain, and stress fields. The dispersal of isotropy in the polymeric density field surrounding the almost spherical silica nanoparticle becomes apparent at the onset of plasticity, with the emergence of a new low-density region and microscopic voids or cavities within the polymer matrix. The evolution of the polymeric density profile clearly shows the exit of atoms from the interphase region once the strain is increased beyond the point of plastic behavior. This is also evident in the onset of a significant reduction in the number of adsorbed chains and the concurrent significant increase in the number of free chains occurring at the elastic-to-plastic transition. In the local strain field, the emergence of an inflection point in the local versus global strain diagram serves as a key indicator of the transition, representing the yield strain (limit of the elastic regime) for each region connected with the breakdown of the compatible deformation condition. The heterogeneities of the local strain are pronounced in the plastic regime. Decomposing the atomic Virial stress into bonded and pair/non-bonded interactions, for nanocomposites with various volume percentages (loading) of the nanoparticles allowed us to probe the influence of the micromechanical environment introduced by the NP in the different types of stress. The rigidity of the material is mainly defined by the non-bonded interactions, which depend strongly on the volume percentage, the lower volume percentage being closer to bulk-like behavior. The introduction of the nanoparticle into the polymer matrix changes the dynamical segmental behavior of the polymer chains, as is evident in the bond stress and the distribution of the length of the Kuhn segments (2-mer vectors).

Our findings highlight the fundamental importance of the microstructural and micromechanical environment at the polymer-nanoparticle interface during tensile strain, offering exciting avenues for future research. Promising directions include exploring the impact of various combinations of polymer-nanoparticle chemistry and surface functionalization on the elastic-to-plastic transition and probing the correlation between strain and density heterogeneities.

Acknowledgements

This project received funding from the European Union's Horizon 2020 research and innovation programme under the Marie Skłodowska–Curie grant agreement No. 101030430. The work was supported by the computational time granted from the Greek Research & Technology Network (GR-NET) in the National HPC facility ARIS under a project named NANOMEC. The work was also supported by CyI High Performance Computing Facility (HPCF) under a project named NANOMEC. The authors acknowledge support by project "SimEA," funded by the European Union's Horizon 2020 research and innovation programme under Grant Agreement No. 810660.

Conflict of Interest

The authors declare no conflict of interest.

Data Availability Statement

The data that support the findings of this study are available on request from the corresponding author. The data are not publicly available due to privacy or ethical restrictions.

Keywords

atomistic simulations, elastic-to-plastic transition, multi-scale modeling, mechanical behavior, polymer nanocomposites

Received: July 27, 2024
Revised: September 4, 2024
Published online: September 18, 2024

[1] J. Berriot, H. Montes, F. Lequeux, D. Long, P. Sotta, *Macromolecules* **2002**, *35*, 9756.
[2] D. Maillard, S. Kumar, B. Fragneaud, J. Kysar, A. Rungta, B. Benicewicz, H. Deng, L. Brinson, J. Douglas, *Nano Lett.* **2012**, *12*, 3909.
[3] A. Papon, H. Montes, F. Lequeux, J. Oberdisse, K. Saalwächter, L. Guy, *Soft Matter* **2012**, *8*, 4090.
[4] J. D. Ferry, H. S. Myers, *J. Electrochem. Soc.* **1961**, *108*, 142C.
[5] H. Reda, A. Chazirakis, A. F. Behbahani, N. Savva, V. Harmandaris, *Nano Lett.* **2023**, *24*, 148.
[6] H. D. Wagner, R. A. Vaia, *Mater. Today* **2004**, *7*, 38.
[7] G. Schmidt, M. M. Malwitz, *Curr. Opin. Colloid Interface Sci.* **2003**, *8*, 103.
[8] F. Hussain, M. Hojjati, M. Okamoto, R. E. Gorga, *J. Compos. Mater.* **2006**, *40*, 1511.
[9] L. Bokobza, *Polymer* **2007**, *48*, 4907.
[10] R. A. Riggleman, H.-N. Lee, M. D. Ediger, J. J. de Pablo, *Soft Matter* **2010**, *6*, 287.
[11] R. A. Riggleman, H.-N. Lee, M. D. Ediger, J. J. de Pablo, *Phys. Rev. Lett.* **2007**, *99*, 21.
[12] J.-L. Barrat, J. Baschnagel, A. Lyulin, *Soft Matter* **2010**, *6*, 3430.
[13] G. J. Papakonstantopoulos, R. A. Riggleman, J.-L. Barrat, J. J. de Pablo, *Phys. Rev. E* **2008**, *77*, 4.
[14] H. Reda, A. Chazirakis, A. J. Power, V. Harmandaris, *J. Phys. Chem. B* **2022**, *126*, 7429.
[15] H. Reda, A. Chazirakis, N. Savva, J.-F. Ganghoffer, V. Harmandaris, *Int. J. Solids Struct.* **2022**, *256*, 111977.
[16] I. M. Ward, D. W. Hadley, *An Introduction to the Mechanical Properties of Solid Polymers*, **1993**.
[17] R. N. Haward, *The Physics of Glassy Polymers*, Springer Science & Business Media, New York, NY **2012**.
[18] J. G. Williams, *Ellis Horwood Limited, Market Cross House, Cooper St, Chichester, West Sussex, PO 19, 1 EB, UK, 1984. 302* **1984**.
[19] R. F. Landel, L. E. Nielsen, *Mechanical Properties of Polymers and Composites*, CRC Press, Boca Raton, FL **1993**.
[20] H. H. Meijer, L. L. Govaert, *Macromol. Chem. Phys.* **2003**, *204*, 274.
[21] R. N. Haward, R. J. Young, editors, *The Physics of Glassy Polymers*, Springer Netherlands, Heidelberg **1997**.
[22] E. Klompen, T. Engels, R. Janssen, L. Govaert, H. Meijer, in *11th International Conference on Fracture 2005, ICF11*, vol. *7*, **2005** pp. 5503–5507.
[23] H. E. Meijer, L. E. Govaert, *Prog. Polym. Sci.* **2005**, *30*, 915.
[24] R. S. Hoy, M. O. Robbins, *J. Polym. Sci., Part B: Polym. Phys.* **2006**, *44*, 3487.
[25] R. S. Hoy, M. O. Robbins, *Phys. Rev. E* **2008**, *77*, 3.
[26] R. S. Hoy, C. S. O'Hern, *Phys. Rev. E* **2010**, *82*, 4.
[27] T. Ge, M. O. Robbins, *J. Polym. Sci., Part B: Polym. Phys.* **2010**, *48*, 1473.
[28] M. Warren, J. Rottler, *Phys. Rev. Lett.* **2010**, *104*, 205501.
[29] M. Warren, J. Rottler, *J. Chem. Phys.* **2010**, *133*, 16.
[30] G. N. Toepperwein, K. S. Schweizer, R. A. Riggleman, J. J. de Pablo, *Macromolecules* **2012**, *45*, 8467.

[31] A. V. Lyulin, J. Li, T. Mulder, B. Vorselaars, M. Michels, *Macromol. Symp.* **2006**, *237*, 108.
[32] R. A. Riggleman, K. S. Schweizer, J. J. d. Pablo, *Macromolecules* **2008**, *41*, 4969.
[33] D. J. Lacks, M. J. Osborne, *Phys. Rev. Lett.* **2004**, *93*, 255501.
[34] Y. G. Chung, D. J. Lacks, *Macromolecules* **2012**, *45*, 4416.
[35] P. Zhu, J. Lin, R. Xiao, H. Zhou, *J. Mech. Phys. Solids* **2022**, *168*, 105046.
[36] E. Kröner, *Arch. Ration. Mech. Anal.* **1959**, *4*, 273.
[37] D. Mathiesen, D. Vogtmann, R. B. Dupaix, *Mech. Mater.* **2014**, *71*, 74.
[38] K. Nayak, D. J. Read, T. C. B. McLeish, P. J. Hine, M. Tassieri, *J. Polym. Sci., Part B: Polym. Phys.* **2011**, *49*, 920.
[39] J. Jancar, R. S. Hoy, A. J. Lesser, E. Jancarova, J. Zidek, *Macromolecules* **2013**, *46*, 9409.
[40] H. van Melick, L. Govaert, H. Meijer, *Polymer* **2003**, *44*, 2493.
[41] J. Kalfus, A. Detwiler, A. J. Lesser, *Macromolecules* **2012**, *45*, 4839.
[42] P. Sathyanarayana, G. Shariff, M. Thimmegowda, M. Ashalatha, R. Ramani, C. Ranganathaiah, *Polym. Int.* **2002**, *51*, 765.
[43] A. C. Rodrigues, M. T. Viciosa, F. Danède, F. Affouard, N. T. Correia, *Mol. Pharmaceutics* **2014**, *11*, 112.
[44] K. Chen, K. S. Schweizer, *Europhys. Lett. (EPL)* **2007**, *79*, 26006.
[45] K. Chen, K. S. Schweizer, *Phys. Rev. Lett.* **2009**, *102*, 3.
[46] K. Chen, K. S. Schweizer, *Macromolecules* **2011**, *44*, 3988.
[47] Y. Zhao, J. Liu, X. Li, Y. Lu, S.-Q. Wang, *Macromolecules* **2017**, *50*, 2024.
[48] S. Herasati, L. C. Zhang, H. H. Ruan, *Int. J. Solids Struct.* **2014**, *51*, 1781.
[49] Y. Li, G. D. Seidel, *Modelling Simul. Mater. Sci. Eng.* **2014**, *22*, 025023.
[50] K. N. Spanos, S. K. Georgantzinos, N. K. Anifantis, *Compos. B. Eng.* **2014**, *63*, 85.
[51] E. N. Skountzos, D. G. Tsalikis, P. S. Stephanou, V. G. Mavrantzas, *Macromolecules* **2021**, *54*, 4470.
[52] S. Pfaller, M. Rahimi, G. Possart, P. Steinmann, F. Müller-Plathe, M. Böhm, *Comp. Meth. Appl. Mech. Eng.* **2013**, *260*, 109.
[53] T. Le, J. Guilleminot, C. Soize, *Comp. Meth. Appl. Mech. Eng.* **2016**, *303*, 430.
[54] G. J. Papakonstantopoulos, M. Doxastakis, P. F. Nealey, J. J. d. Pablo, J.-L. Barrat, *Phys. Rev. E, Stat. Phys., Plasm., Fluids, Relat. Interdisciplin. Top.* **2007**, *75*, 3.
[55] H. Reda, A. Chazirakis, A. F. Behbahani, N. Savva, V. Harmandaris, *Comp. Meth. Appl. Mechan. Eng.* **2022**, *395*, 114905.
[56] G. Odegard, T. Gates, K. Wise, C. Park, E. Siochi, *Compos. Sci. Technol.* **2003**, *63*, 1671.
[57] M. Z. Rong, M. Q. Zhang, Y. Liu, G. C. Yang, H. M. Zeng, *Compos. Sci. Technol.* **2001**, *61*, 1437.
[58] S. W. Shang, J. W. Williams, K. J. M. Söderholm, *J. Mater. Sci.* **1994**, *29*, 2406.
[59] L. Gong, I. A. Kinloch, R. J. Young, I. Riaz, R. Jalil, K. S. Novoselov, *Adv. Mater.* **2010**, *22*, 2694.
[60] G. Anagnostopoulos, C. Androulidakis, E. N. Koukaras, G. Tsoukleri, I. Polyzos, J. Parthenios, K. Papagelis, C. Galiotis, *ACS Appl. Mater. Interfaces* **2015**, *7*, 4216.
[61] P. H. T. Vollenberg, D. Heikens, *Polymer* **1989**, *30*, 1656.
[62] C. L. Wu, M. Q. Zhang, M. Z. Rong, K. Friedrich, *Compos. Sci. Technol.* **2005**, *65*, 635.
[63] L. Zhu, K. A. Narh, *J. Polym. Sci. Pol. Phys.* **2004**, *42*, 2391.
[64] A. F. Behbahani, A. Rissanou, G. Kritikos, M. Doxastakis, C. Burkhart, P. Polińska, V. A. Harmandaris, *Macromolecules* **2020**, *53*, 6173.
[65] R. Tannenbaum, M. Zubris, K. David, D. Ciprari, K. Jacob, I. Jasiuk, N. Dan, *J. Phys. Chem. B* **2006**, *110*, 2227.
[66] K. Baek, H. Park, H. Shin, S. Yang, M. Cho, *Compos. Sci. Technol.* **2021**, *206*, 108673.
[67] V. Kovačević, M. Leskovac, S. L. Blagojević, *J. Adhes. Sci. Technol.* **2002**, *16*, 1915.
[68] P. G. Bolhuis, A. A. Louis, J.-P. Hansen, *Phys. Rev. Lett.* **2002**, *89*, 128302.
[69] K. A. Carrado, L. Xu, *Chem. Mater.* **1998**, *10*, 1440.
[70] K. Johnston, V. Harmandaris, *Soft Matter* **2013**, *9*, 6696.
[71] S. Saber-Samandari, A. A. Khatibi, in *Fracture of Materials: Moving Forwards*, Trans Tech Publications Ltd, Stafa-Zurich **2006**, pp. 199–204.
[72] P. Lu, Y. W. Leong, P. K. Pallathadka, C. B. He, *Int. J. Eng. Sci.* **2013**, *73*, 33.
[73] M. Talò, B. Krause, J. Pionteck, G. Lanzara, W. Lacarbonara, *Compos. B. Eng.* **2017**, *115*, 70.
[74] Z. S. Petrović, W. Zhang, I. Javni, *Biomacromolecules* **2005**, *6*, 713.
[75] M. Alubaidy, K. Venkatakrishnan, B. Tan, A. Mahmood, *J. Nanotechnol. Eng. Med.* **2010**, *1*, 041016.
[76] E. Chabert, M. Bornert, E. Bourgeat-Lami, J.-Y. Cavaillé, R. Dendievel, C. Gauthier, J. L. Putaux, A. Zaoui, *Mater. Sci. Eng. A* **2004**, *381*, 320.
[77] M. Rahimi, I. Iriarte-Carretero, A. Ghanbari, M. C. Böhm, F. Müller-Plathe, *Nanotechnology* **2012**, *23*, 305702.
[78] H.-B. Zhang, W.-G. Zheng, Q. Yan, Z.-G. Jiang, Z.-Z. Yu, *Carbon* **2012**, *50*, 5117.
[79] K. Johnston, V. Harmandaris, *Macromolecules* **2013**, *46*, 5741.
[80] J. Choi, H. Shin, S. Yang, M. Cho, *Compos. Struct.* **2015**, *119*, 365.
[81] S. Yu, S. Yang, M. Cho, *Polymer* **2009**, *50*, 945.
[82] A. F. Behbahani, S. M. V. Allaei, G. H. Motlagh, H. Eslami, V. A. Harmandaris, *Macromolecules* **2018**, *51*, 7518.
[83] A. F. Behbahani, G. H. Motlagh, S. M. V. Allaei, V. A. Harmandaris, *Macromolecules* **2019**, *52*, 3825.
[84] E. Voyiatzis, M. Rahimi, F. Müller-Plathe, M. C. Böhm, *Macromolecules* **2014**, *47*, 7878.
[85] A. Rissanou, H. Papananou, V. Petrakis, M. Doxastakis, K. Andrikopoulos, G. Voyiatzis, K. Chrissopoulou, V. Harmandaris, S. Anastasiadis, *Macromolecules* **2017**, *50*, 6273.
[86] C. Wu, *J. Phys. Chem. B* **2011**, *115*, 11044.
[87] H. Reda, A. Chazirakis, A. F. Behbahani, N. Savva, V. Harmandaris, *MethodsX* **2022**, *9*, 101931.

